Depth Resolution Enhancement Technique for CMOS Time-of-Flight 3-D Image Sensors

Mohamed Lamine Hafiane, Wilfried Wagner, Zohir Dibi, and Otto Manck

***Abstract*— Introducing Time-of-Flight 3-D image sensors to actual engineering applications, such as pattern recognition, is constrained not only by their limited depth and lateral resolution, but also by how similar the precision of depth measurement throughout the whole pixel-matrix is. In real operating environment, an observed 3-D-scene hardly exhibits a homogeneous reflectance factor. Moreover, the light-beam (laser source) presents a nonuniform optical power distribution in space. Thus, the amount of the incident light on the sensor surface varies drastically from one pixel to another, and so does the signal-to-noise ratio. To address this problem, this paper investigates the impact of both scene and light-source non-ideal characteristics on the sensor performance. An adaptive on-pixel analog signal processing technique is also presented and applied to the design of a 32 × 32 complementary metal oxide semiconductor (CMOS) range camera, featuring an interesting cost-efficient solution.**

***Index Terms*— Analog averaging, beam optical power distribution, CMOS image sensor, correlated double sampling, multiple double short time integration principle, objects reflectance, time-of-flight.**

I. Introduction

SMART machine vision with accurate perception of the third dimension (3-D image) is required in a growing number of applications, ranging from everyday human-computer interfacing to complex robotic guidance, automotive and security [1–10]. Stereovision (combining two ordinary passive cameras) is the commonly used technique; however, this technique is conditioned by the image processing task, which is still an open issue, particularly point matching in different views. Recently, ToF range camera has received more attention, since it offers an image acquisition rate akin to that of stereovision techniques, with a relatively accurate depth resolution and wide distance range measurement, extending from a few centimeters up to tens of meters. Well-known successful implementations of ToF range camera are carried out using the indirect time-of-flight technique, which requires a relatively low-speed signal processing, compared to direct time-of-flight measurement. Generally, 3-D image sensors based on indirect ToF can be achieved with less than 5% relative depth precision, using one of the two main derived techniques: pulse ToF or phase shift determination [7–15; 20–21]. From the implementation viewpoint, the most promising reported works have been achieved using standard CMOS process, as they exhibit relatively low power consumption and the integration of various digital/analog signal processing, on the same silicon-die, leading to a highly cost-efficient implementation compared to CCD-based implementations.

In principle, an observed scene is irradiated with a light beam, featuring a narrow wavelength bandwidth. The 3-D image is then virtually reconstructed from a finite number of range pixels. Each pixel measures the distance (traveling time) from the sensor toward its corresponding area in the observed scene (pixel projected area). However, the incident light power on the sensor surface (reflected beam) depends strongly on the optical and geometrical features of a given observed scene. Furthermore, the employed light beam (laser) exhibits a non-homogeneous power distribution, generally Gaussian-like [16]. Thereby, the relative signal-to-noise ratio diverges from one pixel to another, depending upon the characteristics of both 3-D scene and the beam source. This gives rise to a large pixel-to-pixel dissimilarity (measurement precision), and thus corrupting the 3-D image integrality. Although, complex optical solutions are employed to reduce the non-homogeneous of the beam (optical power distribution); the impact of the optical/geometric features of the scene on the sensor performance cannot be eliminated. It is therefore, a challenging task to maintain an acceptable measurement precision level throughout the matrix pixels.

From another aspect, the inherent image fixed pattern noise (*FPN*), resulting from devices non-ideality and mismatch, also introduces a significant pixel-to-pixel non-uniformity. Unlike the dissimilarity in measurement precision, however, these non-uniformities do not depend explicitly on the sensor operating conditions, and thus are relatively easy to reduce using various soft/hardware techniques.

The present work is part of a larger effort to introduce ToF range cameras to real applications, by enhancing their robustness against operating environment, while keeping an acceptable trade-off between performances and implementa-

Manuscript received July 1, 2011; revised January 16, 2012; accepted February 3, 2012. Date of publication February 7, 2012; date of current version April 27, 2012. This work was done by the Optotransmitter-Umweltschutz-Technologie e.V. and the Technical University of Berlin. This work was supported by the Development Program INNO-WATT of the Bundesministerium für Wirtschaft und Technologie, and in part by the Iris GmbH. The associate editor coordinating the review of this paper and approving it for publication was Dr. Sandro Carrara.

M. L. Hafiane and O. Manck are with the Institut für Technische Informatik und Mikroelektronik, Technische Universität Berlin, Berlin D-10587, Germany (e-mail: hafiane_lamine@mikro.ee.tu-berlin.de; manck@mikro.ee.tu-berlin.de).

W. Wagner is with Optotransmitter-Umweltschutz-Technologie, Berlin 12555, Germany (e-mail: wagner@out-ev.de).

Z. Dibi is with the Laboratoire d'Electronique Avancee, University of Batna, Batna 05000, Algeria (e-mail: zohirdibi@yahoo.fr).

Color versions of one or more of the figures in this paper are available online at http://ieeexplore.ieee.org.

Digital Object Identifier 10.1109/JSEN.2012.2187350

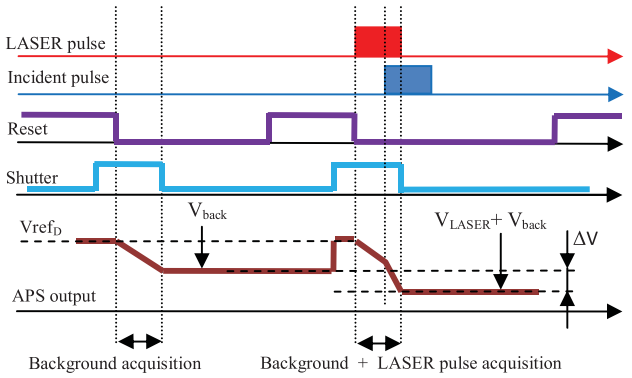

Fig. 1. Sketch of the APS timing diagram.

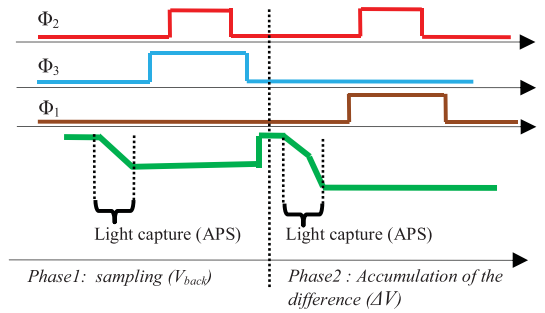

Fig. 2. Sketch of the CDS and accumulation timing diagram.

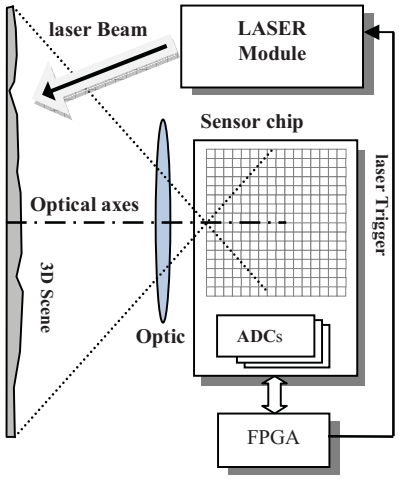

Fig. 3. 3-D-image sensor.

tion cost. The main points addressed by the present paper are as follows: first, we introduce the design and operating principle of a CMOS 3-D-image sensor. An analytical analysis of the sensor *SNR* is presented, in which the impact of the sensor operating conditions (optical/geometric) is emphasized. We also investigate the advantages and drawbacks of the implementation of an on-pixel analog averaging technique to enhance the *SNR*. The 3-D-image homogeneity, in terms of depth resolution from one pixel to another, is then examined through an appropriate analysis based on experimental results.

II. Sensor Design and Operating Principle

The 3-D-image sensor was developed based on the indirect time-of-flight technique, with its derived algorithm: multiple double short time integration (MDSI); in the literature, it may also refer to the so-called pulse time-of-flight. This technique generally presents two interesting advantages: high robustness against background irradiance, and relatively low required energy for the light beam (laser pulse with roughly a 0.1% duty cycle) [7–9, 12–13, 17]. The sensor core (chip) was implemented using 0.6μm standard CMOS technology, allowing the integration, within the same silicon-die, of several analog/digital circuits; among other, on-pixel analog signal processing, four ADCs to provide digital outputs, and current/voltage references. The digital signal processing, including the 3-D-image recovery, was performed using an off-chip FPGA. The whole 3-D image sensor comprises a sensor chip, an off-chip FPGA, an adequate optics module (lens system) and a laser source (Figs. 3 and 7).

The proposed pixel architecture, depicted in Fig. 4, consists of a double active pixel sensor (APS-A and -B), correlated double sampling (*CDS*), analog averaging (switched capacitors integrator), and sample & hold stage. This structure is derived from successful implementation techniques of pulse time-of-flight, adopted in the late 1990s and the 2000s, based on similar techniques developed originally for CMOS-based imaging [7–9, 12–13]. The proposed pixel exhibits however, the particularity of sharing one analog processing stage (CDS/Analog averaging) between two APSs leading to a relative improved fill factor. Basically, an APS with electronic shutter and analog memory (C_0) allows extremely rapid light capture (a few tens of nanoseconds). As illustrated in the timing diagram of Fig. 1, a typical measurement frame is performed twice, without and then with laser pulse. The difference is then taken as the output signal (ΔV), using the *CDS* stage, leading to an efficient suppression of all unwanted offsets such as: diode reset voltage ($Vref_D$), source follower offset, background-light, and dark-current, due to the leakage current of the reverse-bias diode (temperature dependent). For single laser-pulse capture, a high-speed shutter window (reset OFF/shutter ON) is synchronized with the laser-pulse emission. At the end of this period (shutter OFF), the residual voltage is then stored in the hold-capacitor (C_0). This voltage exhibits in principle a linear variation with respect to the traveling time, assuming both laser and background irradiance are time invariant.

In real applications, the laser source has a limited optical power, imposed by eye-safety requirements and/or the electrical power budget. In addition, the reflected laser power is severely declined, especially for long distance measurements [17]. From another aspect, it is generally assumed that CMOS image sensors suffer from more noise than CCD-based sensors [17–19]. Hence, the CMOS-ToF range camera presents an inherent faint *SNR*. This drawback can be overcame, however, by introducing an analog averaging technique (on-pixel SC integrator). This technique is widely used in CMOS 3-D-image sensors [7–9, 12–13]. In principle, the resulting voltage differences (without/with laser pulse) are accumulated N times in analog memory (C_{1a}/C_{1b}). Provided that, the target remains static during the whole measurement process, the signal level increases by a factor of N, while the noise level (*rms*) increases only by a factor of $\sqrt{N}$, since the noise present at each accumulation step is uncorrelated with the noise present in

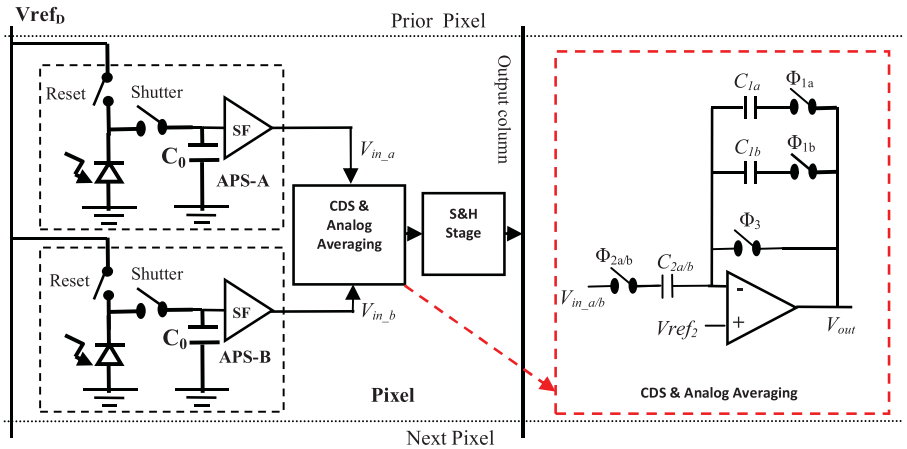

Fig. 4. Pixel scheme.

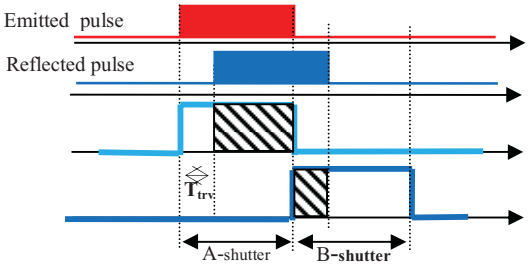

Fig. 5. Timing sketch of the double shutter technique.

other steps. The *SNR* is thus enhanced by a factor of $\sqrt{N}$ (analog averaging).

The diagram of a typical accumulation cycle, either for APS-A or -B, is sketched in Fig. 2. It consists of two phases, sampling and accumulation, where each phase is synchronized with the corresponding APS phase (Fig. 1). First, the APS outputs (V_{in_a}/V_{in_b}) are sampled in the input capacitors (C_{2a}/C_{2b}). In the coming phase, the APS output ($V_{LASER} + V_{back}$) is subtracted from the value previously stored (V_{back}), and the difference ($\Delta V = V_{LASER}$) is accumulated (in $C_{1a/b}$). So, both *CDS* and analog averaging are implemented within one sub-circuit (switched capacitors). Note that, both sampling and accumulation phases are performed after the light measurement (APS).

The voltages stored in $C_{1a/b}$ are completely independent from the background illumination and the sensor temperature as well. However, they are a function of the employed laser pulse power, object reflectance and the sensor intrinsic parameters. These independencies are further suppressed using the double shutter technique. As illustrated in Fig. 5, the technique consists of using two equal and consecutive shutter windows (integration period), with $T_{Ashutter} = T_{Bshutter} = T_{pulse}$. The resulting voltages (for *N acc.*) are given by Eq. (1) and (2) for A and B respectively.

$$V_A = N \times \frac{AS_{ph0}}{C_{int}}[E_{LASER}(T_{shutter} - T_{trv})] \quad (1)$$

$$V_B = N \times \frac{AS_{ph0}}{C_{int}}[E_{LASER}(T_{trv})] \quad (2)$$

where, C_{int} is the integration capacitor (diode junction capacitor parallel to C_0), S_{ph0} is the photodiode sensitivity at the laser wavelength (Ampere/Watt), A is The photodiode area, E_{LASER} is the incident laser power per area-unit (irradiance); on the sensor surface. $T_{shutter}$ is the width of the integration window, and $T_{trv}$is the traveling time. Hence, the traveling time can be deduced as follows:

$$T_{trv} = T_{pulse}\left[\frac{V_B}{V_B + V_A}\right]. \quad (3)$$

III. Problem Formulation and Signal-to-Noise Ratio

As mentioned before, a ToF range camera operating in a real environment exhibits high dissimilarity in measurement precision from one pixel to another. This dissimilarity is proportional to the signal-to-noise ratio, which is the starting point of the conducted analysis. The *SNR* for a given pixel, related to the reflected laser pulse, is expressed as follows:

$$SNR_{LASER} = 20\log\left(\sqrt{N} \times \frac{AS_{ph0}E_{LASER}(T_{shutter} - T_{trv})}{\sqrt{\overline{V_n^2}}C_{int}}\right) \quad (4)$$

while for B-APS is given by:

$$SNR_{LASER} = 20\log\left(\sqrt{N} \times \frac{AS_{ph0}E_{LASER}(T_{trv})}{\sqrt{\overline{V_n^2}}C_{int}}\right) \quad (5)$$

with $\sqrt{\overline{V_n^2}}$ is the *rms* (root mean square value) of the equivalent noise. Assuming that, the target area irradiated by the laser source coincides with the sensor field-of-view, the incident laser irradiance can then be expressed as:

$$E_{LASER} = r \times \frac{P_0}{A_{prt}} \quad (6)$$

where P_0 corresponds to the peak-power of the LASER-pulse (source). Note that, the mean power remains relatively low, as the duty cycle rarely exceeds 0.1% (MDSI principle). A_{prt}

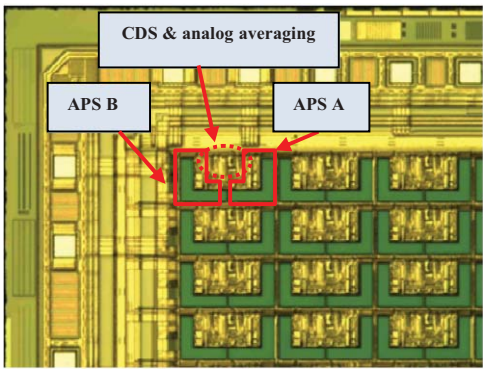

Fig. 6. Part of the silicon-die microphotograph.

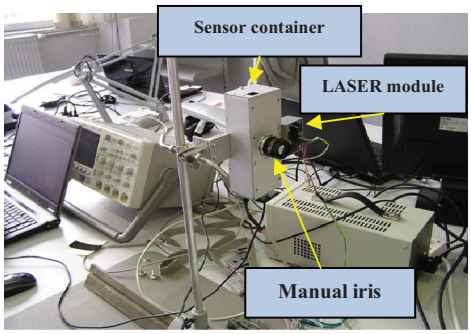

Fig. 7. Sensor photograph.

is the matrix projected area on the observed scene (function of the lens characteristics and target distance), and r is the reflection factor (<1). For distances much larger than the lens focal-length, the projected matrix area (A_{prt}) and the reflection factor (r) are given as follows:

$$A_{prt} = A_{MAT}\left(\frac{d}{f}\right)^2 \tag{7}$$

$$r \approx \rho k\left(\cos(\theta)\right)^2 \times \frac{1}{4 \times f_{\#}^2} \tag{8}$$

whith, f is the focal length (lenses), d is the target distance from the sensor, ρ is the reflectivity of a given object surface, k is the optical loss factor, θ is the surface inclination with respect to the optical axis, $f_{\#}$ is the f-number ($f_{\#} = f/R$, R the aperture diameter), A_{MAT} is the matrix area, and the factor "4" refers to Lambert reflector.

From Eq. (4) to (6) the signal-to-noise ratio is rearranged to give Eq. (9) and (10) for A- and B-APS respectively.

$$SNR_{LASER} = 20\log\left(\sqrt{N} \times \frac{rP_0}{A_{prt}} \times \frac{AS_{ph0}(T_{shutter} - T_{trv})}{\sqrt{\overline{V_n^2}C_{int}}}\right) \tag{9}$$

$$SNR_{LASER} = 20\log\left(\sqrt{N} \times \frac{rP_0}{A_{prt}} \times \frac{AS_{ph0}(T_{trv})}{\sqrt{\overline{V_n^2}C_{int}}}\right). \tag{10}$$

This formulation emphasizes the limit of the sensor measurement precision, in terms of random uncertainty. In this sense, the *SNR* is limited by the inherent noise floor ($\sqrt{\overline{V_n^2}}$), the object reflection factor (r) and the laser power budget (P_0). However, increasing the number of accumulations (analog averaging) enhances, theoretically, the *SNR* and so the relative precision.

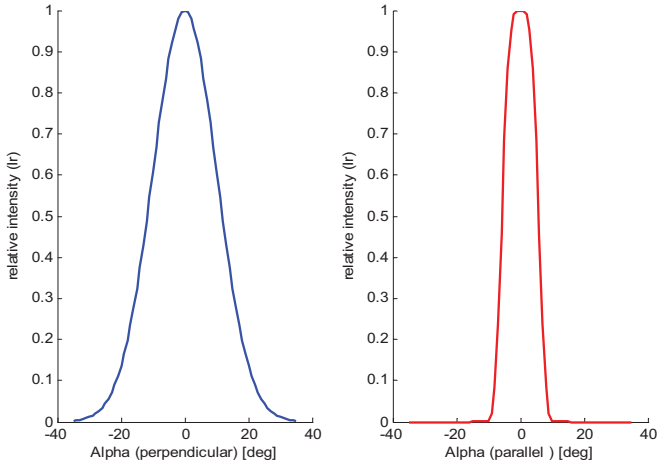

Fig. 8. Beam far-field distribution, perpendicular/parallel to laser diode junction.

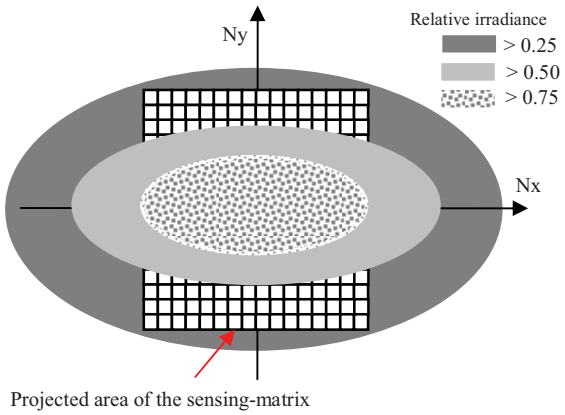

Fig. 9. Relative irradiance distribution on a flat area located at 1 m.

IV. Measurement Results and Analysis

Fig. 6 depicts a portion of the silicon-die microphotograph, where the basic pixel sub-circuits can be clearly distinguished (highlighted areas). The sensor chip (prototype) presented in this paper, was fabricated using 0.6μm standard CMOS process. The sensor chip is part of a whole system dedicated to 3-D imaging (Fig. 7).

A. Non-Homogeneous Optical Power Distribution

In practice, all kinds of laser beam exhibit a non-homogeneous optical power distribution, with most optical power is generally concentrated near to the beam's geometrical center. Usually, a Gaussian profile describes most common distributions. Even so, there are more elaborated profiles, for instance flat top, obtained by means of complex optical systems, or by combining several light sources, up to tens of LEDs [20], [21]; it is difficult, however, to achieve standard

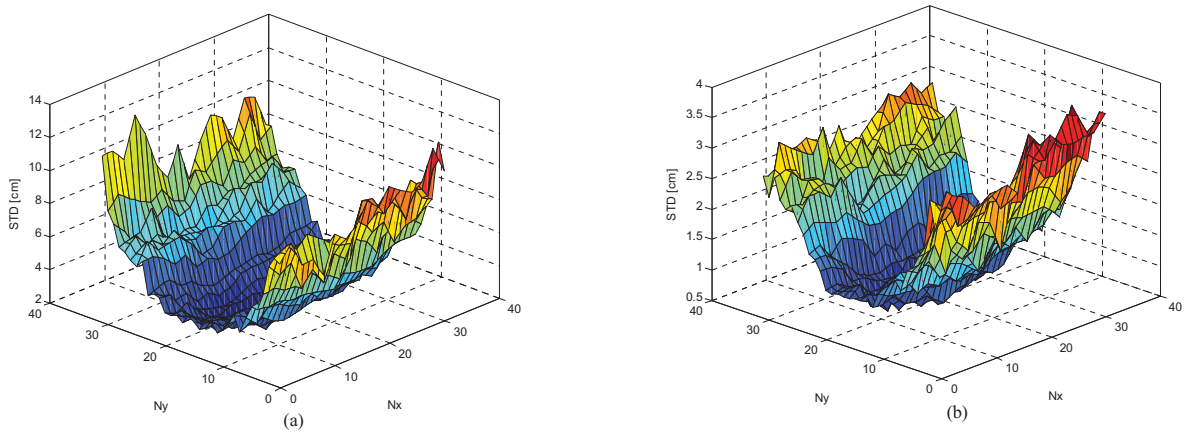

Fig. 10. Standard deviation (1σ) throughout the whole matrix (flat white target/1 m). (a) 50 acc and (b) 200 acc.

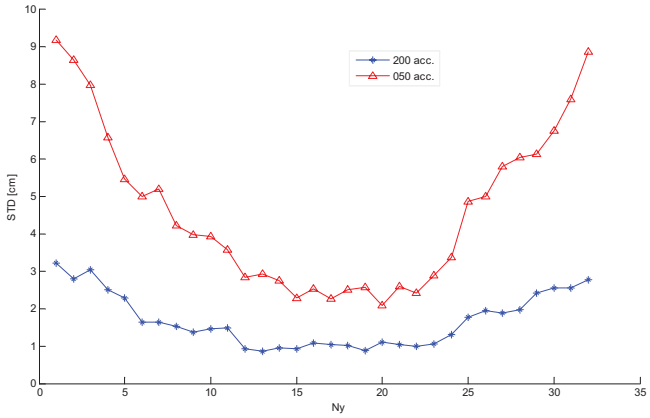

Fig. 11. Standard deviation throughout the column of number 16 (flat white target/1 m).

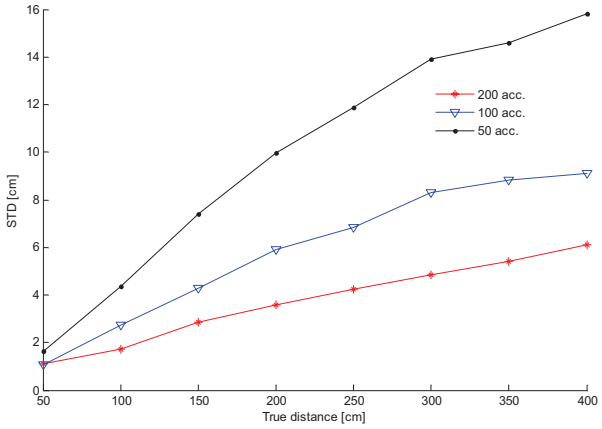

Fig. 12. Standard deviation versus distance for different numbers of accumulations.

solutions with cost-efficient, low power consumption, acceptable power efficiency (electrical-to-optical), and to meet eye-safety requirements as well. Furthermore, the optical module has to handle a short-pulse signal (a few tens of nanoseconds), giving rise thus to the possibility of optic interferences, due to poor synchronization or unwanted reflections, especially when using multiple laser-sources.

Considering, in first approach, a flat target with uniform reflectivity characteristic. The signal-to-noise ratio, according to Eq. (9) and (10), is proportional to the laser power, and thus the measurement precision, throughout the pixel-matrix, is expected to exhibit a correlated variation to the optic power distribution profile. Fig. 8 illustrates an example of a relative intensity (I_{ref}) distribution of a laser beam as a function of the divergence angle (alpha perpendicular/ parallel); in addition, Fig. 9 sketches the expected relative laser irradiance on a flat area located 1 meter from the sensor, as well as the pixel-matrix projected area (at the same location). The standard deviation (*std*) of the distance measurement, evaluated for each pixel based-on 255 samples and with a different number of accumulations, is depicted in Fig. 10 (3-D pattern of std). For a better illustration, Fig. 11 shows in addition, the variation in std across column 16 (center of the matrix), of the same results. These results highlight two main points: the optical power distribution profile leads to a significant variation in terms of measurement precision, and the std floor is reduced from about 12 cm for 50 accumulations to about 4 cm for 200 accumulations (Fig. 10(a) *vs.* Fig. 10(b)), which points out to the effectiveness of the on-pixel analog averaging technique. It should be mentioned that, the relative test configuration does not correspond to standard operating conditions, as an actual scene is far from being a simple flat white target; further, each employed laser beam exhibits a unique Far-field distribution (Fig. 8). However, the conducted analysis, based-on the experiment results, provides a general overview of the non-homogeneous power distribution impact on the sensor performance, whereby, any particular situation can be predicted.

B. Non-Homogeneous Reflectivity

An actual observed-scene is unlikely to have a uniform surface and/or a homogeneous reflectivity coefficient (ρ). Hence, the amount of the incident optical power (reflected laser pulse) fluctuates from one pixel to another, and so the distance measurement precision exhibits a significant pixel-to-pixel dissimilarity, as can be inferred from the experimental results reported in table 1. The results are relative to the central pixel (line: 16, column: 16), with the target is placed 1m away

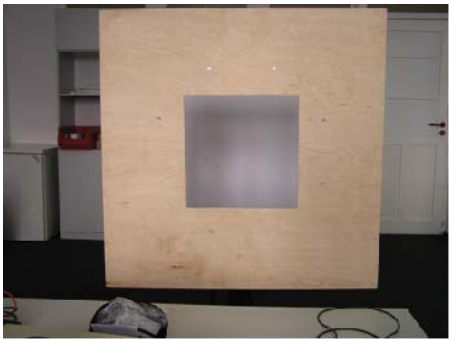

Fig. 13. Target photograph.

TABLE I
SENSOR PRECISION FOR DIFFERENT TARGET BACKGROUND

Target	STD [cm] (1σ/ 255 samples)	Mean ρ (Estimated)
White	1.4	> 0.70
Gray	2.2	≈ 0.50
Black	14.6	< 0.10

from the sensor, and the measurement is performed using 200 accumulations (analog averaging).

From these results, the precision throughout the sensor pixels (matrix), for a given observed scene exhibiting a non-homogeneous reflectance factor, can thus be drawn, as the precision fluctuates dramatically, roughly by a factor of ten, from white to black background. Similar to the impact of the beam non-homogeneity on the sensor depth resolution, the non-homogeneous reflectivity also gives rise to a large dissimilarity in distance precision.

C. Precision Versus Distance (Relative Error)

Obviously, all telemetry-based distance measurement presents a given limit to the relative precision. For 3-D image sensors, however, this limit gives rise to a particular concern, regarding the recovery of the 3-D-data when a given scene contains objects with sharp-depth (edges). As two points, with different location with respect to the sensor, are not detected with similar precision, which limits the sensor applicability, especially for pattern recognition.

In ToF based 3-D image sensor, the issue of the relative precision is multiple. From one aspect, according to Eq. (4) the *SNR* decreases with respect to the traveling time; considering 90 % of the distance range ($T_{trv} = 0.9T_{shutter}$), the *SNR* is reduced by a factor of 10 [17]. Furthermore, due to the divergence nature of all light beams, the reflected laser irradiance drops with the distance from the source, following the well-known inverse square law. Hence, the *SNR* is drastically diminished as the distance increases.

A typical standard-deviation (1σ / 255 samples) as a function of distance for different numbers of accumulations is depicted in Fig. 12; the reported results refer to the central pixel and flat white target. As can be deduced, the on-pixel analog averaging reduces the measurement uncertainty range between the short and long distances, which leads to a significant improvement in terms of depth information extraction and recognition, especially when a given observed scene contains objects with sharp edges, as further illustrated in Section V.

V. DEPTH DATA RECOVERY

It has been shown so far how the on-pixel analog averaging (SC-integrator) significantly improves the depth resolution. Although the accumulation process is carried out locally for each pixel (parallel signal processing), increasing the number of accumulations reduces the image acquisition speed. For instance, the sensor presented here operates with a typical acquisition rate of 20 kHz (50 us for one accumulation cycle), and thus for 100 accumulations the rate is about 200 frames/second. This represents an adequate acquisition rate for an image consisting of 1024 range-pixels, compared to other reported works, which use a similar 3-D imaging technique [7–9].

In a real operating environment, part of an observed scene, not necessarily the entire scene, may exhibit a very low reflectance factor, such as dark objects (absorbing rather reflecting the laser-wavelength), sharp edges, and surfaces with high tilt angle (relative to the optical axis). The signal-to-noise ratio is drastically degraded for the corresponding pixels, and thus the needed number of accumulations increases steeply. On the other hand, other pixels may have a relatively high signal-to-noise ratio (for the same observed scene), giving rise to a possible pixel-output saturation for a higher number of accumulations. Hence, an adapted number of accumulations is required. This can be achieved by probing the pixel output and comparing it with a given reference, the saturation flag is then used to stop the accumulation process.

In addition to the depth measurement precision and the image acquisition rate, the lateral resolution (pixel count) is also a deterministic feature for many applications involving range cameras. However, ToF-3-D image sensors still exhibit a low lateral resolution compared to the standard 2-D image, since the on-pixel analog processing solution limits the pixel fill-factor from one side, and the sensitive area required to detect the reflected laser pulse, especially for long distances and/or objects with a low reflectance.

The inherent 3-D image fixed-pattern-noise (*FPN*), due to the pixel-to-pixel mismatch (signal path), as well as the distance measurement nonlinearities are reduced using various calibration techniques; among others lookup table, which presents a relatively easy way for 3-D data mapping and requires a realistic computing time for data processing. The image optic distortion is corrected using trigonometric calibration, by knowing the exact coordinates (X, Y, Z) of each point and the lens characteristics. Moreover, the ToF range camera, based-on MDSI technique, allows an efficient suppression of temperature and background-light, as reported by many arts [7–9, 12].

An illustrative test target is shown in Fig. 13. It consists of a flat board, with a square hole, placed 50 cm in front of a standard wall, while the sensor is placed at 3m away from the target. Fig. 14 illustrates a typical 3-D mapping of the target, before and after eliminating *FPN*. The 3-D-image was reconstructed based-on the distance data, collected from each

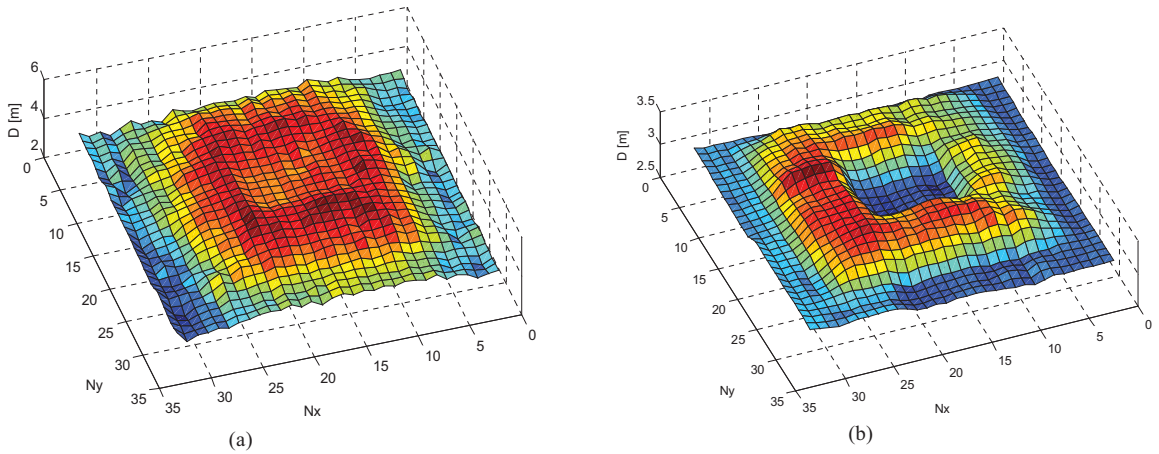

Fig. 14. Target 3-D image (200 acc). (a) Before eliminating FPN. (b) After eliminating FPN.

pixel. The results show the ability of the sensor to recover the depth data, even when the scene contains sharp edges (such as a square hole), which is an important feature for many engineering applications, based on ToF cameras, such as automotive.

VI. Conclusion

CMOS-based ToF-3-D image sensor presents a cost efficient solution for various range-imaging applications, due to the opportunity of integrating on-pixel analog signal processing, which leads to a significant enhancement in terms of image depth resolution. Although on-pixel analog processing reduces the pixel fill-factor, a good compromise, considering realistic operating conditions, between the overall depth measurement precision, the pixel count (lateral resolution) and the image acquisition rate can be found. However, standard solutions are not yet available, since the sensor performances are still conditioned by the features of a given observed scene. Furthermore, increasing the lateral resolution by scaling down the range-pixel size requires the usage of higher laser optical power to achieve extreme operating environment (dark objects located at long distance range). As the optic-sensing area shrinks (scaling down), and the shutter time (integration window) for MDSI-3-D sensor rarely exceeds a few tens of nanoseconds, the signal-to-noise ratio remains relatively low compared to the standard 2-D image sensor. This represents the main challenge and issue facing the CMOS-ToF range camera.

Acknowledgment

The authors would like to thank to A. Thun, CEO of IRIS GmbH, Berlin.

References

[1] K. C. Fuerstenberg and K. Dietmayer, "Object tracking and classification for multiple active safety and comfort applications using a multilayer laser scanner," in *Proc. IEEE Intell. Vehicles Symp.*, Jun. 2004, pp. 802–807.

[2] S. B. Gokturk and C. Tomasi, "3-D head tracking based on recognition and interpolation using a time-of-flight depth sensor," in *Proc. IEEE Comput. Vision Pattern Recognit.*, Jun.–Jul. 2004, pp. 211–217.

[3] S. Hsu, S. Acharya, A. Rafii, and R. New, "Performance of a time-of-flight range camera for intelligent vehicle safety applications," in *Proc. Adv. Microsyst. Automot. Applicat.*, 2006, pp. 205–219.

[4] P. Breuer, C. Eckes, and S. Müller, "Hand gesture recognition with a novel IR time-of-flight range camera-a pilot study," in *Proc. Comput. Vision/Comput. Graphics Collaborat. Tech.*, 2007, pp. 247–260.

[5] S. Acharya, C. Tracey, and A. Rafii, "System design of time-of-flight range camera for car park assist and backup application," in *Proc. IEEE Comput. Vision Pattern Recognit. Workshops Comput. Soc. Conf.*, Anchorage, AK, Jun. 2008, pp. 1–6.

[6] L. Sabeti, E. Parvizi, and Q. M. J. Wu, "Visual tracking using color cameras and time-of-flight range imaging sensors," *J. Multimedia*, vol. 3, no. 2, pp. 28–36, Jun. 2008.

[7] P. Mengel, L. Listl, B. König, C. Toepfer, M. Pellkofer, W. Brockherde, B. Hosticka, O. Elkhalili, O. Schrey, and W. Ulfig, "3-D CMOS image sensor pedestrian protection collision mitigation," in *Proc. Conf. Adv. Microsyst. Automot. Applicat.*, 2006, pp. 1–23.

[8] O. Elkhalili, O. M. Schrey, P. Mengel, M. Petermann, W. Brockherde, and B. J. Hosticka, "A 4 × 64 pixel CMOS image sensor for 3-D measurement applications," *IEEE J. Solid-State Circuits*, vol. 39, no. 7, pp. 1208–1212, Jul. 2004.

[9] O. Elkhalili, O. M. Schrey, W. Ulfig, W. Brockherde, B. J. Hosticka, P. Mengel, and L. Listl, "A 64 × 8 pixel 3-D CMOS time of flight image sensor for car safety applications," in *Proc. Conf. IEEE Solid-State Circuits*, Montreaux, Switzerland, Sep. 2006, pp. 568–571.

[10] A. Kolb, E. Barth, R. Koch, and R. Larsen, "Time-of-flight sensors in computer graphics," in *State-of-the-Art Report*. Aire-la-Ville, Switzerland: Eurographics Association, 2009, pp. 119–134.

[11] S. A. GuOmundsson, H. Aanaes, and R. Larsen, "Environmental effects on measurement uncertainties of time-of-flight cameras," in *Proc. Int. Symp. Signals Circuits Syst.*, Jul. 2007, pp. 1–4.

[12] M. Perenzoni, N. Massari, D. Stoppa, L. Pancheri, M. Malfatti, and L. Gonzo, "A 160 × 120-pixels range camera with in-pixel correlated double sampling and nonuniformity correction in 29.1 μm pitch," in *Proc. IEEE Conf. Solid-State Circuits*, Sep. 2010, pp. 294–297.

[13] L. Viarani, D. Stoppa, L. Gonzo, M. Gottardi, and A. Simoni, "A CMOS smart pixel for active 3-D vision applications," *IEEE Sensors J.*, vol. 4, no. 1, pp. 145–152, Feb. 2004.

[14] S. Kawahito, I. A. Halin, T. Ushinaga, T. Sawada, M. Homma, and Y. Maeda, "A CMOS time-of-flight range image sensor with gates-on-field-oxide structure," *IEEE Sensors J.*, vol. 7, no. 12, pp. 1578–1586, Dec. 2007.

[15] R. Lange, P. Seitz, A. Biber, and R. Schwarte, "Time-of flight range imaging with a custom solid state image sensor," *Proc. SPIE*, vol. 3823, no. 1, pp. 180–191, 1999.

[16] J. Alda, "Laser and Gaussian beam propagation and transformation," *Encyclopedia Opt. Eng.*, pp. 999–1013, Sep. 2003.

[17] M. L. Hafiane, W. Wagner, Z. Dibi, and O. Manck, "Analysis and estimation of NEP and DR in CMOS TOF-3D image sensor based on MDSI," *Sensors Actuat. A: Phys.*, vol. 169, no. 1, pp. 66–73, 2011.

[18] M. Bigas, E. Cabruja, J. Forest, and J. Salvi, "Review of CMOS image sensors," *Microelectron. J.*, vol. 37, no. 5, pp. 433–451, May 2006.

[19] H. Tian, B. Fowler, and A. E. Gamal, "Analysis of temporal noise in CMOS photodiode active pixel sensor," *IEEE J. Solid-State Circuits*, vol. 36, no. 1, pp. 92–101, Jun. 2001.
[20] T. Kahlmann, F. Remondino, and H. Ingensand, "Calibration for increased accuracy of the range imaging camera SWISSRANGER," in *Proc. Symp. Image Eng. Vision Metrol.*, 2006, pp. 137–141.
[21] T. Oggier, B. Büttgen, F. Lustenberger, G. Becker, B. Rüegg, and A. Hodac, "SwissRanger SR3000 and first experiences based on miniaturized 3D-TOF cameras," in *Proc. 1st Range Imag. Res.*, 2005, pp. 1–12.

Mohamed Lamine Hafiane received the Engineering degree (Diplom-Ingenieur) in electronic measurement and control and the Magister degree in integrated circuit (IC)-design from the University of Batna, Batna, Algeria, in 2003 and 2006, respectively.

He has been a Research Fellow with the Technical University of Berlin, Berlin, Germany, since 2006, where he worked in the field of IC-design, and has been an Analog IC Designer for many Germany-based companies, such as MAZ-gmbh, Berlin, and IRIS-gmbh, Berlin. His current research interests include analog IC-designs and intelligent microsensors.

Wilfried Wagner received the Diplom degree in physics from Humboldt-University Berlin, Berlin, Germany, and the Ph.D. degree in 1979.

He was a member of the Liquid Crystal Research Group, Academic Institute of Elektronenphysik Berlin, Berlin, from 1974 to 1990. From 1994 to 1998, he was with the Technical University of Berlin, Berlin, where he worked in the field of the molecular-statistical theory of liquid crystals. In 2002, he joined Optotransmitter-Umweltschutz-Technologie e.V., Berlin, and he is now the Head of the Sensor Group. His current research interests include complementary metal-oxide-semiconductor photosensors and 3-D-imaging.

Zohir Dibi received the Electronics Engineering degree from the University of Setif, Setif, Algeria, in 1989, and the M.Eng. and Ph.D. degrees in microelectronics from the University of Constantine, Constantine, Algeria, in 1998 and 2004, respectively.

He has been the Head of the Electronics Department, Batna University, Batna, Algeria, since 1993, where he is currently an Assistant Professor. His current research interests include neuronal networks, sensors, and smart sensors.

Otto Manck received the Diplom degree in physics and the Ph.D. degree in numeric device modeling from RWTH Aachen University, Aachen, Germany.

He was a Follower with the Institute of Theoretical Electromechanics, RWTH Aachen University, from 1969 to 1978. From 1978 to 1983, he was with the IC Development Center, AEG-Telefunken Company, Berlin, Germany. In 1983, he founded the Institute of Microelectronics, Technical University of Berlin, Berlin, where he is a Research Adviser. His current research interests include application-specific integrated circuits development methodology.